

# Charge transfer fluctuation, $d$ -wave superconductivity, and the $B_{1g}$ Raman phonon in the Cuprates: A detailed analysis

T. P. Devereaux<sup>1</sup>, A. Virosztek<sup>2,3</sup> and A. Zawadowski<sup>3,2</sup>

<sup>1</sup>*Department of Physics, University of California, Davis, CA 95616*

<sup>2</sup>*Research Institute for Solid State Physics, POB 49, H-1525 Budapest, Hungary*

<sup>3</sup>*Institute of Physics, Technical University of Budapest, H-1521 Budapest, Hungary*

The Raman spectrum of the  $B_{1g}$  phonon in the superconducting cuprate materials is investigated theoretically in detail in both the normal and superconducting phases, and is contrasted with that of the  $A_{1g}$  phonon. A mechanism involving the charge transfer fluctuation between the two oxygen ions in the  $\text{CuO}_2$  plane coupled to the crystal field perpendicular to the plane is discussed and the resulting electron-phonon coupling is evaluated. Depending on the symmetry of the phonon the weight of different parts of the Fermi surface in the coupling is different. This provides the opportunity to obtain information on the superconducting gap function at certain parts of the Fermi surface. The lineshape of the phonon is then analyzed in detail both in the normal and superconducting states. The Fano lineshape is calculated in the normal state and the change of the linewidth with temperature below  $T_c$  is investigated for a  $d_{x^2-y^2}$  pairing symmetry. Excellent agreement is obtained for the  $B_{1g}$  phonon lineshape in  $\text{YBa}_2\text{Cu}_3\text{O}_7$ . These experiments, however, can not distinguish between  $d_{x^2-y^2}$  and a highly anisotropic  $s$ -wave pairing.

PACS numbers: 74.20.-z, 74.20.Fg, 74.25.Gz, 74.25.Kc, 74.72.-h  
(Received June 25, 2021)

## I. INTRODUCTION

As a result of the recent dispute as to whether the superconducting gap in the high- $T_c$  materials is  $s$ - or  $d$ -type all experiments which can contribute to resolve that question are of special importance [1]. It was shown recently [2] that the study of the polarization dependence of the electronic Raman scattering can address these questions and can distinguish between the different orientations ( $d_{x^2-y^2}$  or  $d_{xy}$ ) of the gap as well. This evidence can be made more complete by including the phonons and the effect of the electron-phonon coupling, which is the subject of the present paper [3].

The analysis of the lineshape of optical phonons in the high  $T_c$  superconductors has been the focus of a large body of investigation [4,5]. Of the many Raman active modes in tetragonal superconductors, all the modes that have been observed in the cuprate materials using in-plane polarizations transform according the  $A_{1g}$  symmetry except one, which transforms according to  $B_{1g}$  symmetry [5]. Since this phonon obeys its own selection rules, the frequency of the mode can be unambiguously assigned, which is in contrast with the early confusion of the assignments of the separate  $A_{1g}$  modes.

In this paper the phonons involving the perpendicular vibrations of the in-plane oxygens are investigated. The displacements of the two oxygens O(2) and O(3) are in phase for  $A_{1g}$  symmetry and out of phase for  $B_{1g}$  as is shown on Fig. (1) for the case of  $\text{YBa}_2\text{Cu}_3\text{O}_y$ . The coupling of these phonons to the electrons in the plane has an interesting feature, namely a completely flat  $\text{CuO}_2$  plane taken out of the surrounding atomic environment has the mirror symmetry through the plane. Thus the linear coupling between these phonons and the in-plane electrons is absent. In a crystal however, as it has first been pointed out by Barišić *et.al.* [6], that symmetry can be broken since there is an electric field perpendicular to the plane due to the surrounding ions forming an asymmetric environment. This is in contrast to the La compound, where only the small tilting of the octahedra breaks the symmetry [7]. The perpendicular electric field in the 1:2:3 material can be responsible for the buckling of the  $\text{CuO}_2$  plane, i.e. the slight separation of the planes formed by the Cu and O ions. This small distortion however cannot be responsible for the large electron-phonon coupling to be discussed here.

Since the long-range charge transfer fluctuations between unit cells are screened, only intracell charge transfers must be considered. Let us denote the charge transfer fluctuations at O(2) and O(3) by  $\delta\rho_x$  and  $\delta\rho_y$  (see Fig. 1.) respectively. A charge transfer fluctuation where  $\delta\rho_x - \delta\rho_y \neq 0$  is obviously coupled to the electric field and the crystal deforms in

the form of the  $B_{1g}$  phonon, similarly  $\delta\rho_x + \delta\rho_y \neq 0$  is coupled to the  $A_{1g}$  phonon. The fluctuations of the in-plane charges are either due to the transfer (i) between the in-plane oxygens and other ions, or (ii) between the two in-plane oxygens. The fluctuations of the  $A_{1g}$  symmetry  $\delta\rho_x = \delta\rho_y$  can be a consequence of the transfers between the in-plane copper and oxygens. For  $B_{1g}$  symmetry both (i) and (ii) may be realized.

Considering the first possibility [8], the charge transfer in 1:2:3 between the bridging oxygen O(4) and the O(3) is a good candidate. As long as the non-bonding orbital of O(4) parallel to the CuO chain has a partial electronic density of states near the Fermi surface, the transfer breaks the  $x - y$  symmetry. That mechanism, which is sensitive to the position of the electronic partial density of states of the bridging oxygen relative to the Fermi energy, has been worked out in detail [8], but the recently observed Raman spectra are not consistent with the predicted  $d_{xy}$  superconducting gap [2].

The second possibility does not depend on such details of the electronic band structure, since only the conduction band plays a role. The charge transfer fluctuation  $\delta\rho_x + \delta\rho_y = 0$  between O(2) and O(3) involves especially those parts of the cylindrical Fermi surface which are close to the  $k_x$  and  $k_y$  axis. Thus the influence of the electron-phonon coupling on the electronic Raman continuum depends strongly on whether a large superconducting gap opens at that part of the Fermi surface. More precisely, the electronic contribution can be characterized by the azimuthal quantum number  $m$  on the cylindrical Fermi surface [3,9], and  $m = \pm 2$  corresponds to  $B_{1g}$  symmetry, while out of the two ( $m = 0$ ,  $m = \pm 4$ ) channels of  $A_{1g}$  symmetry only  $m = \pm 4$  is relevant since the  $m = 0$  mode describes charge fluctuations between cells, which are screened by the long-range Coulomb interaction. The different Fermi surface areas probed by Raman scattering in the  $A_{1g}$  and  $B_{1g}$  geometry are illustrated in Fig. (2). ( $A_{1g}$  and  $B_{1g}$  transforms like  $\cos(4\phi)$  and  $\cos(2\phi)$  respectively). Thus assuming a  $d_{x^2-y^2}$  type superconducting gap the  $B_{1g}$  mode probes the areas with the largest gap, while the  $A_{1g}$  averages the areas of both the largest gap and the nodes. The most appropriate tool in the Raman experiments to probe the electron-phonon coupling is to study the Fano interference which is formed due to the simultaneous scattering of light on the phonons and the electronic continuum (see eg. Refs. [4] and [8]). The fit of the Fano lineshape provides information not only on the coupling but also on the electronic continuum influenced by the opening of the superconducting gap. The appearance of a sharper gap in the  $B_{1g}$  symmetry than in the  $A_{1g}$  provides a unique identification of the gap of  $d_{x^2-y^2}$  type [2]. It must be emphasized however, that these experiments are not sensitive to the sign of the order parameter, therefore can not distinguish between  $d$ -wave superconductivity and a

very highly anisotropic  $s$  type.

The present status of the relation between experiment and theory can be summarized as follows. The vibration of the  $B_{1g}$  mode which appears at roughly 340 wavenumbers in all cuprate materials, is connected with the antisymmetric out-of-plane vibrations of the O(2) and O(3) ions in the Cu-O plane [5]. The net charge transfer of this vibration in the unit cell is zero and thus the long range Coulomb forces are incapable of screening the charge fluctuations. Consequently, the mode has a large cross section for scattering incoming photons and thus appears in Raman experiments as a large sharp signal centered at frequency shifts corresponding to the energy of the mode. Due to the strength and unambiguous identification of the mode, the  $B_{1g}$  phonon has been lavished with attention [5]. In particular, the spectral lineshape of the mode has been a subject of intense scrutiny both in the normal and superconducting state of the cuprates. In the normal state, the asymmetry of the lineshape indicates strong mixing of the phonon with the electronic continuum and fits to a Breit-Wigner or Fano lineshape have been made with great success [4]. This has usually led to the assertion that the electron-phonon coupling at least for this mode is large. However no estimates of the coupling from a microscopic theory have been presented except for the theoretical suggestion by Barišić and Kupčić [6]. Further, the anomalous changes of the  $B_{1g}$  phonon as the material enters into the superconducting state have also been exhaustively documented [4,5,10]. The temperature dependence of the changes in the  $B_{1g}$  phonon's lineshape have been used to help determine the magnitude of the energy gap of the superconductor [10]. Recently, a theory of Raman scattering in  $d$ -wave superconductors has been presented [2,3] and while the general features of the theory fit well with the experiment, no detailed fit of the lineshape could be made without further knowledge of the mechanism and strength of the electron-phonon coupling.

In the present paper we provide a detailed theory for the behavior of the  $B_{1g}$  phonon in both the normal and superconducting states of the cuprate materials using the mechanism suggested by Barišić *et.al.* [6,7]. In particular, we investigate the mechanism of electron-phonon coupling resulting from crystal field effects and describe the Fano lineshape in the normal state. The theory is then generalized to the superconducting state and the lineshape is calculated in detail for a superconductor with  $d_{x^2-y^2}$  pairing.

The paper is organized as follows. In Sec. II. we develop the mechanism which leads to first order electron-phonon coupling due to the presence of the crystal field. Based on the 3-band model for the CuO<sub>2</sub> plane the electron-phonon coupling constant is evaluated. In Sec. III. we apply these results in order to fit the experimental data in the normal state.

Particular attention is paid to the Fano resonance. Section IV. is devoted to the behavior of the phonon lineshape in the superconducting state. Here we show that the temperature dependence of the spectrum is due to the change in the electronic response, and the data are consistent with a  $d_{x^2-y^2}$  gap. Finally our conclusions are given in Sec. V.

## II. MECHANISM

In the first part of this section we define our model for the electrons in the  $\text{CuO}_2$  plane. This allows us to introduce notations used in the second part, where we develop a microscopic theory of the coupling of these electrons to the out-of-plane phonons due to the crystal field perpendicular to the plane.

### A. The model

Using the notations of Ref. [11] we consider the 3-band model for the  $\text{CuO}_2$  plane described by the following Hamiltonian:

$$H^0 = \varepsilon \sum_{\mathbf{n},\sigma} b_{\mathbf{n},\sigma}^\dagger b_{\mathbf{n},\sigma} + t \sum_{\mathbf{n},\boldsymbol{\delta},\sigma} P_{\boldsymbol{\delta}} (b_{\mathbf{n},\sigma}^\dagger a_{\mathbf{n}+\boldsymbol{\delta}/2,\sigma} + h.c.), \quad (1)$$

where  $b_{\mathbf{n},\sigma}^\dagger$  creates an electron with spin  $\sigma$  at a copper lattice site  $\mathbf{n}$ , while  $a_{\mathbf{n},\boldsymbol{\delta},\sigma}$  annihilates an electron at one of the neighboring oxygen sites  $\mathbf{n} + \boldsymbol{\delta}/2$  determined by the unit vector  $\boldsymbol{\delta}$  assuming the four values,  $(\pm 1, 0)$  and  $(0, \pm 1)$ . An oxygen atom between the two copper atoms at sites  $\mathbf{n}$  and  $\mathbf{n} + \boldsymbol{\delta}$  is labeled by either  $(\mathbf{n}, \boldsymbol{\delta})$  or  $(\mathbf{n} + \boldsymbol{\delta}, -\boldsymbol{\delta})$ . Moreover,  $\varepsilon = E_d - E_p$  is the difference of the Cu and O site energies,  $t$  is the Cu-O hopping integral and  $P_{\boldsymbol{\delta}} = \pm 1$  depending on whether the orbitals (with real wavefunctions) have the same or opposite sign at the overlap region. Assuming Cu  $d_{x^2-y^2}$  and O  $p$  orbitals  $P_{-\boldsymbol{\delta}} = -P_{\boldsymbol{\delta}}$ , and we can choose  $P_{(1,0)} = 1$  and  $P_{(0,1)} = -1$ . For simplicity, we neglect direct O-O hopping.

The momentum representation is defined by the following formulae:

$$b_{\mathbf{n},\sigma} = \frac{1}{\sqrt{N}} \sum_{\mathbf{k}} e^{i\mathbf{k}\cdot\mathbf{n}} b_{\mathbf{k},\sigma}, \quad (2)$$

and

$$a_{\mathbf{n},\boldsymbol{\delta},\sigma} = \frac{1}{\sqrt{N}} \sum_{\mathbf{k}} \exp[i\mathbf{k}\cdot(\mathbf{n} + \boldsymbol{\delta}/2)] a_{\mathbf{k},\boldsymbol{\delta},\sigma}, \quad (3)$$

where  $a$  is the lattice constant,  $N$  is the number of Cu sites and  $\alpha$  is  $x$  or  $y$  for  $\boldsymbol{\delta} = (\pm 1, 0)$  and  $\boldsymbol{\delta} = (0, \pm 1)$  respectively. In this representation the Hamiltonian in Eq.(1) decouples for different momenta as

$$H^0 = \sum_{\mathbf{k}, \sigma} H_{\mathbf{k}, \sigma}^0, \quad (4)$$

where

$$H_{\mathbf{k}, \sigma}^0 = \varepsilon b_{\mathbf{k}, \sigma}^\dagger b_{\mathbf{k}, \sigma} + \{i b_{\mathbf{k}, \sigma}^\dagger [a_{x, \mathbf{k}, \sigma} t_x(\mathbf{k}) - a_{y, \mathbf{k}, \sigma} t_y(\mathbf{k})] + h.c.\}, \quad (5)$$

and

$$t_\alpha(\mathbf{k}) = 2t \sin(ak_\alpha/2). \quad (6)$$

$H_{\mathbf{k}, \sigma}^0$  is then easily diagonalized as

$$H_{\mathbf{k}, \sigma}^0 = \sum_{\beta} E_{\beta}(\mathbf{k}) d_{\beta, \mathbf{k}, \sigma}^\dagger d_{\beta, \mathbf{k}, \sigma}, \quad (7)$$

where  $\beta$  assumes the values  $+$ ,  $-$ , and  $0$  for the antibonding, bonding, and nonbonding bands, respectively. The corresponding electronic energies are  $E_0(\mathbf{k}) = 0$  and

$$E_{\pm}(\mathbf{k}) = \varepsilon/2 \pm \sqrt{(\varepsilon/2)^2 + \Omega^2(\mathbf{k})}, \quad (8)$$

with

$$\Omega^2(\mathbf{k}) = t_x^2(\mathbf{k}) + t_y^2(\mathbf{k}). \quad (9)$$

The transformation between the original  $(a, b)$  and the new  $(d)$  electronic operators is described by

$$\begin{pmatrix} b \\ a_x \\ a_y \end{pmatrix} = (\mathbf{e}_+, \mathbf{e}_0, \mathbf{e}_-) \begin{pmatrix} d_+ \\ d_0 \\ d_- \end{pmatrix}, \quad (10)$$

where the column vectors of the transformation matrix are given by

$$\mathbf{e}_0 = \frac{1}{\Omega} \begin{pmatrix} 0 \\ t_y \\ t_x \end{pmatrix}, \quad (11)$$

and

$$\mathbf{e}_{\pm} = \frac{1}{\sqrt{E_{\pm}^2 + \Omega^2}} \begin{pmatrix} E_{\pm} \\ -it_x \\ it_y \end{pmatrix}. \quad (12)$$

In the last three equations we have dropped the  $\mathbf{k}, \sigma$  indices for clarity.

In the physically relevant situation for the  $\text{CuO}_2$  plane the upper band is close to half filled. Since the three bands do not overlap in the present model, we will consider only a reduced one-band Hamiltonian describing the upper band and neglect the bonding and nonbonding bands. Then the reduced Hamiltonian is given by

$$H_{red}^0 = \sum_{\mathbf{k}, \sigma} E(\mathbf{k}) d_{\mathbf{k}, \sigma}^{\dagger} d_{\mathbf{k}, \sigma}, \quad (13)$$

with

$$E(\mathbf{k}) = \varepsilon/2 + \sqrt{(\varepsilon/2)^2 + \Omega^2(\mathbf{k})}. \quad (14)$$

Furthermore, the expressions of the transformation from  $d$  operators to  $a$  and  $b$  operators reduce to

$$b_{\mathbf{k}, \sigma} = \phi_b(\mathbf{k}) d_{\mathbf{k}, \sigma}, \quad (15a)$$

$$a_{x, \mathbf{k}, \sigma} = \phi_x(\mathbf{k}) d_{\mathbf{k}, \sigma}, \quad (15b)$$

$$a_{y, \mathbf{k}, \sigma} = \phi_y(\mathbf{k}) d_{\mathbf{k}, \sigma}, \quad (15c)$$

where

$$\phi_b(\mathbf{k}) = E(\mathbf{k}) [E^2(\mathbf{k}) + \Omega^2(\mathbf{k})]^{-1/2}, \quad (16a)$$

$$\phi_x(\mathbf{k}) = -it_x(\mathbf{k}) [E^2(\mathbf{k}) + \Omega^2(\mathbf{k})]^{-1/2}, \quad (16b)$$

$$\phi_y(\mathbf{k}) = it_y(\mathbf{k}) [E^2(\mathbf{k}) + \Omega^2(\mathbf{k})]^{-1/2}. \quad (16c)$$

As we will see in the next subsection, this simple model contains the most important ingredients in order to describe the electron-phonon coupling.

## B. Electron-phonon coupling

As we have discussed already, the electrons in the  $\text{CuO}_2$  plane do not couple in first order to the phonon modes with displacement vectors perpendicular to the plane, because in that case the hopping integrals change only in second order in the displacements. However, if there is an electric field perpendicular to the plane, first order electron-phonon coupling is generated. In our case this field originates from the asymmetric environment around the  $\text{CuO}_2$  plane (see Fig.1.), and is also responsible for the buckling of the plane with restoring force provided by the covalent bonds.

Let us consider the effect of a lattice periodic crystal field  $\mathbf{E}(\mathbf{r}) = -\nabla\phi_{ext}(\mathbf{r})$  on the electrons in the plane. The electron density at each (displaced) site couples to the external field via the Hamiltonian

$$\begin{aligned} H' = & -e \sum_{\mathbf{n},\sigma} \{ b_{\mathbf{n},\sigma}^\dagger b_{\mathbf{n},\sigma} \phi_{ext}[\mathbf{a}\mathbf{n} + \mathbf{u}_b(\mathbf{a}\mathbf{n})] \\ & + a_{\mathbf{n},\mathbf{x},\sigma}^\dagger a_{\mathbf{n},\mathbf{x},\sigma} \phi_{ext}[\mathbf{a}\mathbf{n} + \mathbf{a}\mathbf{x}/2 + \mathbf{u}_x(\mathbf{a}\mathbf{n})] \\ & + a_{\mathbf{n},\mathbf{y},\sigma}^\dagger a_{\mathbf{n},\mathbf{y},\sigma} \phi_{ext}[\mathbf{a}\mathbf{n} + \mathbf{a}\mathbf{y}/2 + \mathbf{u}_y(\mathbf{a}\mathbf{n})] \}, \end{aligned} \quad (17)$$

where  $\mathbf{u}_b(\mathbf{a}\mathbf{n})$ ,  $\mathbf{u}_x(\mathbf{a}\mathbf{n})$ , and  $\mathbf{u}_y(\mathbf{a}\mathbf{n})$  are displacement vectors of the Cu, O(2), and O(3) in the unit cell at the lattice site  $\mathbf{n}$ ,  $e$  is the electron charge, and  $\mathbf{x}$  and  $\mathbf{y}$  are unit vectors in the corresponding directions. Expansion in the displacements up to first order leads to

$$H' = H'_{site} + H_{el-ph} + \dots, \quad (18)$$

where  $H'_{site}$  renormalizes the copper-oxygen site energy difference  $\varepsilon$  only, while the term linear in  $\mathbf{u}$  generates an electron-phonon interaction

$$\begin{aligned} H_{el-ph} = & e \sum_{\mathbf{n},\sigma} \{ \mathbf{E}_b \mathbf{u}_b(\mathbf{a}\mathbf{n}) b_{\mathbf{n},\sigma}^\dagger b_{\mathbf{n},\sigma} \\ & + \mathbf{E}_x \mathbf{u}_x(\mathbf{a}\mathbf{n}) a_{\mathbf{n},\mathbf{x},\sigma}^\dagger a_{\mathbf{n},\mathbf{x},\sigma} \\ & + \mathbf{E}_y \mathbf{u}_y(\mathbf{a}\mathbf{n}) a_{\mathbf{n},\mathbf{y},\sigma}^\dagger a_{\mathbf{n},\mathbf{y},\sigma} \}, \end{aligned} \quad (19)$$

where  $\mathbf{E}_b$ ,  $\mathbf{E}_x$ , and  $\mathbf{E}_y$  are the electric fields at the Cu, O(2), and O(3) sites respectively, which are parallel to the  $z$ -axis due to symmetry. In the absence of chains  $\mathbf{E}_x = \mathbf{E}_y$  would hold.

$H_{el-ph}$  can be written in momentum representation with the help of Eqs.(2-3), and Eq.(15) allows us to express the interaction of phonons and electrons of the reduced Hamiltonian Eq.(13) in the usual form

$$H_{el-ph} = \frac{1}{\sqrt{N}} \sum_{\mathbf{q}, \lambda} \sum_{\mathbf{k}, \sigma} g_{\lambda}(\mathbf{k}, \mathbf{q}) d_{\mathbf{k}+\mathbf{q}, \sigma}^{\dagger} d_{\mathbf{k}, \sigma} [c_{\lambda}(\mathbf{q}) + c_{\lambda}^{\dagger}(-\mathbf{q})]. \quad (20)$$

Here  $c_{\lambda}(\mathbf{q})$  annihilates a phonon mode  $\lambda$  with wavevector  $\mathbf{q}$  and  $g_{\lambda}(\mathbf{k}, \mathbf{q})$  is the coupling constant of that mode to an electron of wavevector  $\mathbf{k}$ . Based on our microscopic model the coupling constant can easily be evaluated using standard procedures of the quantum theory of phonons [12].

In the context of Raman scattering we are interested in  $\mathbf{q} = 0$  optical phonons. In case of the  $B_{1g}$  phonon the Cu displacement is zero, while the O(2) and O(3) atoms have equal and opposite displacements (Fig.1.b). The corresponding coupling constant is evaluated as

$$g_{B_{1g}}(\mathbf{k}, \mathbf{q} = 0) = e \sqrt{\frac{\hbar}{2M_o \omega_{B_{1g}}}} \frac{1}{\sqrt{2}} [(\mathbf{E}_x)_z |\phi_x(\mathbf{k})|^2 - (\mathbf{E}_y)_z |\phi_y(\mathbf{k})|^2], \quad (21)$$

where  $M_o$  is the oxygen mass and  $\omega_{B_{1g}}$  is the phonon frequency. In the following we make the approximation  $(\mathbf{E}_x)_z = (\mathbf{E}_y)_z = E_z$ . Due to the opposite displacements of the oxygens, the *difference* of the  $\phi_{\alpha}$  functions (given by Eq.(16)) determines the  $\mathbf{k}$  dependence of the  $B_{1g}$  coupling. Since  $\Omega(\mathbf{k}) = \text{const.}$  on the Fermi surface (see Eq.(14)), this coupling constant is proportional to  $t_x^2(\mathbf{k}) - t_y^2(\mathbf{k}) \propto \cos(ak_x) - \cos(ak_y)$ , which is clearly of  $B_{1g}$  character. In fact, this is exactly the second order Fermi surface harmonic [13] of our model band structure (Eq.(14)) transforming according to the  $B_{1g}$  symmetry. Therefore we can write the coupling in the form

$$g_{B_{1g}}(\mathbf{k}, \mathbf{q} = 0) = g_{B_{1g}} \phi_{B_{1g}}^{m=2}(\mathbf{k}), \quad (22)$$

where

$$\phi_{B_{1g}}^{m=2}(\mathbf{k}) = \frac{1}{\sqrt{N_{B_{1g}}(E_F)}} [\cos(ak_x) - \cos(ak_y)] \quad (23)$$

is the normalized second order Fermi surface harmonic of  $B_{1g}$  symmetry with the normalization constant at the Fermi energy  $E_F$  given by [13]

$$N_{B_{1g}}(E_F) = \frac{\int d^2k \delta[E_F - E(\mathbf{k})] [\cos(ak_x) - \cos(ak_y)]^2}{\int d^2k \delta[E_F - E(\mathbf{k})]}. \quad (24)$$

All information about the strength of the coupling is now compressed in the expansion coefficient

$$g_{B_{1g}} = -e E_z \sqrt{\frac{\hbar}{2M_o \omega_{B_{1g}}}} \frac{2t^2}{E_F(2E_F - \varepsilon)} \sqrt{\frac{N_{B_{1g}}(E_F)}{2}}. \quad (25)$$

In case of the  $A_{1g}$  phonon the oxygen displacements are the same both in magnitude and in direction (Fig.1.a) and the displacement of the copper is negligible due to the relative rigidity of its vertical bonds. The same procedure employed for the  $B_{1g}$  phonon yields the following coupling constant for the  $A_{1g}$  phonon

$$g_{A_{1g}}(\mathbf{k}, \mathbf{q} = 0) = eE_z \sqrt{\frac{\hbar}{2M_o\omega_{A_{1g}}}} \frac{1}{\sqrt{2}} [|\phi_x(\mathbf{k})|^2 + |\phi_y(\mathbf{k})|^2]. \quad (26)$$

In this case however, the coupling depends on  $\mathbf{k}$  only through the energy  $E(\mathbf{k})$ , i.e. it is constant on the Fermi surface for any band filling. Therefore within the present model the  $A_{1g}$  phonon couples to homogeneous density fluctuations only, and since these fluctuations are suppressed by the long range Coulomb interaction, the resulting coupling is vanishingly small. This conclusion remains valid if we allow for a finite Cu displacement as well [14], but does not necessarily hold if e.g. O-O hopping is included.

At the end of this section we wish to evaluate the coupling in Eq.(25). For a half filled band the Fermi energy  $E_F = \varepsilon/2 + \sqrt{(\varepsilon/2)^2 + (2t)^2}$ , and the normalization constant  $N_{B_{1g}}(E_F) = 4$ . It is reasonable to suppose that  $\varepsilon/2 \ll 2t$ , and in this limit we only need the electric field  $E_z$  at the oxygen site for a numerical value of  $g_{B_{1g}}$ . In order to estimate this field we suppose that the charges on the planes of the unit cell of  $\text{YBa}_2\text{Cu}_3\text{O}_7$  are evenly distributed, and the charges (per unit cell, in units of  $e$ ) for the planes Y, Ba, and  $\text{CuO}_2$  are +3, +2, and -2 respectively, while the remaining (chain) region has -3 electron charge to insure neutrality of the unit cell. Each plane produces an electric field at the oxygen site we are concerned with independent of its distance. Since all planes in the sample contribute, we consider ever larger environments of the  $\text{CuO}_2$  plane in question. We calculate the field produced by the two neighboring (Y and Ba) planes first, then include the next nearest neighbors etc. The series of values for  $E_z$  is of course not convergent, but has a period of the unit cell. Although a more accurate calculation applying the Ewald summation is desirable [7], for an estimate we use the average value in this series, which yields  $eE_z = -2\pi e^2/a^2 = -6.1\text{eV}/\text{\AA}$ . According to Eq.(25) this crystal field generates a coupling  $g_{B_{1g}} = 0.12\text{eV}$ . The relevant dimensionless coupling  $\lambda_{B_{1g}} = N_F g_{B_{1g}}^2 / \hbar\omega_{B_{1g}} = 0.078$  if we use a total density of states at the Fermi level  $N_F = 0.22/\text{eV}$  corresponding to a bandwidth of 9eV. We note here that due to the presence of chains the tetragonal symmetry of the  $\text{CuO}_2$  plane is weakly broken, and  $(\mathbf{E}_x)_z \neq (\mathbf{E}_y)_z$ . This leads to the slight mixing of the  $A_{1g}$  and  $B_{1g}$  modes.

### III. NORMAL STATE

In this section we utilize our calculations for the coupling constant to discuss the resulting spectra of the cuprates in the normal state, while in the next section we discuss the changes in the spectra due to superconductivity.

The inelastic scattering of photons from a metal can either be caused by collisions with phonons or via the creation of electron-hole pairs. As well, the phonons interact with the electronic continuum and have a dynamical effect on the way photons are scattered. The total light scattering cross section resulting from these contributions is depicted by the Feynman diagrams in Fig. 3. The coupling constant  $\gamma$  describes the electron-photon coupling, (i.e., the Raman vertex for particle-hole creation due to the vector potential of the incoming light). In the limit of small momentum transfer and frequency transfers smaller than the optical band gap, the Raman vertex is simply related to the curvature of the band dispersion  $\epsilon(\mathbf{k})$  and the incident ( $\hat{\mathbf{e}}^I$ ) and scattered ( $\hat{\mathbf{e}}^S$ ) polarization light vectors via

$$\gamma(\mathbf{k}) = \frac{m}{\hbar^2} \sum_{\alpha,\beta} e_\alpha^I \frac{\partial^2 \epsilon(\mathbf{k})}{\partial k_\alpha \partial k_\beta} e_\beta^S, \quad (27)$$

which can be expanded in terms of Fermi surface harmonics  $\phi^m(\mathbf{k})$ ,  $\gamma(\mathbf{k}) = \sum_m \gamma_m \phi^m(\mathbf{k})$ . The remaining vertices we denote by  $g_{p-p}$  for the photon-phonon vertex, and  $g_\lambda$  for the electron-phonon vertex as discussed in the previous section. The bare phonon propagator is given by

$$D_\lambda^0(\omega) = \frac{2\omega_\lambda}{\omega^2 - \omega_\lambda^2 + 2i\omega_\lambda \Gamma_\lambda^i}, \quad (28)$$

where  $\Gamma_\lambda^i$  is the intrinsic phonon linewidth resulting from e.g. the decay of the phonon caused by the presence of an anharmonic lattice potential. In the metallic state, the electron-phonon coupling renormalizes the phonon propagator such that

$$D_\lambda(\omega) = \frac{D_\lambda^0(\omega)}{1 + g_\lambda^2 D_\lambda^0(\omega) \chi_\lambda(\omega)}, \quad (29)$$

where  $\chi_\lambda$  is the complex electronic susceptibility evaluated in channel  $\lambda$  [15]. Defining the renormalized phonon frequency through

$$\hat{\omega}_\lambda^2 = \omega_\lambda^2 (1 - \lambda(\omega)), \quad (30)$$

where  $\lambda(\omega) = 2g_\lambda^2 \chi'_\lambda(\omega)/\omega_\lambda$  and  $\chi'$  denotes the real part of the susceptibility, we arrive at the following expression for the renormalized phonon propagator

$$D_\lambda(\omega) = \frac{2\omega_\lambda}{\omega^2 - \hat{\omega}_\lambda^2 + 2i\omega_\lambda\Gamma_\lambda(\omega)}, \quad (31)$$

where  $\Gamma_\lambda$  is the total frequency dependent linewidth of the phonon,  $\Gamma_\lambda(\omega) = \Gamma_\lambda^i + g_\lambda^2\chi_\lambda''(\omega)$ .

We now sum up the diagrams in Fig. (3) for the Raman response in terms of the susceptibility  $\chi_\lambda$ . After some lengthy but trivial algebra we obtain

$$\begin{aligned} \chi_{\lambda,full}''(\omega) = & \frac{(\omega + \omega_a)^2}{(\omega^2 - \hat{\omega}_\lambda^2)^2 + [2\omega_\lambda\Gamma_\lambda(\omega)]^2} \left\{ \gamma_\lambda^2 \chi_\lambda''(\omega) \left[ (\omega - \omega_a)^2 + 4\Gamma_\lambda^i\Gamma_\lambda(\omega) \left( \frac{\omega_\lambda}{\omega + \omega_a} \right)^2 \right] \right. \\ & \left. + 4g_{p-p}^2\Gamma_\lambda^i \left( \frac{\omega_\lambda}{\omega + \omega_a} \right)^2 [1 + \lambda(\omega)/\beta]^2 \right\}, \end{aligned} \quad (32)$$

with

$$\beta = \frac{2g_{p-p}g_\lambda}{\gamma_\lambda\omega_\lambda}, \quad \gamma_\lambda = \langle \phi_\lambda(\mathbf{k})\gamma(\mathbf{k}) \rangle. \quad (33)$$

Here  $\langle \dots \rangle$  denotes an average over the Fermi surface. Thus  $\gamma_\lambda$  represents the symmetry elements of the Raman vertex projected out by the incoming and outgoing photon polarization vectors.

Eq. (32) is a generalized form of the Breit-Wigner or Fano lineshape describing the interaction of a discrete excitation (phonon) with an electronic continuum. Here the frequency  $\omega_a = \omega_\lambda\sqrt{1+\beta}$  sets the position of the antiresonance of the lineshape. If the intrinsic phonon width  $\Gamma_\lambda^i = 0$  then at the antiresonance  $\chi_{\lambda,full}''(\omega = \omega_a) = 0$ . Since  $\chi_\lambda$  describes the electronic contribution to Raman scattering, which is generally featureless and a smooth function of frequency, we can replace everywhere  $\chi_\lambda$  by the value it takes on near the phonon frequency to fit the Raman spectra in the vicinity of the phonon. However to fit the entire spectrum in the normal state, the full  $\omega$  dependence is required.

The description of the continuum in high  $T_c$  superconductors has been the focus of a large body of both theoretical and experimental work. While at present no theory can completely describe the full symmetry-dependent continuum for a large range of frequency shifts, we now give expressions for the continuum in two separate cases. In the presence of impurity scattering, the continuum lineshape has a simple Lorentzian form [16]

$$\chi_\lambda''(\omega) = N_F \frac{\omega\tau_\lambda^{*-1}}{\omega^2 + \tau_\lambda^{*-2}}. \quad (34)$$

Here  $1/\tau_\lambda^* = 1/\tau_{m=0} - 1/\tau_\lambda$  is the channel-dependent impurity scattering rate reduced by vertex corrections. While this form can fit the data on the cuprate materials at least in the  $B_{1g}$  channel (i.e., crossed polarization orientations aligned 45 degrees with respect to the

$a - b$  axis in the Cu-O planes) at low frequencies, the high frequency tail which remains relatively constant and the frequency behavior at low frequencies in other channels cannot be accounted for.

Another form for the continuum can be arrived at by taking nesting of the Fermi surface into account as has been done by one of the present authors [17]. The Raman susceptibility has a similar form as Eq. (34) with the impurity scattering rate replaced by the addition of the electron-electron and impurity scattering rates on a nested Fermi surface and the effect of mass renormalization taken into account,

$$\begin{aligned} \tau_\lambda^{*-1} &\rightarrow \tau_\lambda^{*-1} + \alpha\sqrt{(\beta'T)^2 + \omega^2}, \\ \omega &\rightarrow \omega m^*(\omega)/m, \\ \text{with } m^*(\omega)/m &= 1 + \frac{2\alpha}{\pi} \ln \left[ \frac{\omega_c}{\sqrt{(\beta'T)^2 + \omega^2}} \right], \end{aligned} \quad (35)$$

where  $\alpha, \beta'$  and  $\omega_c$  are constants determined by a fit to the electronic continuum in the normal state. This form for the Raman susceptibility provides an adequate description to the continuum in the normal state of both YBCO and BSCCO (see Ref. [17]) and thus we will use this form rather than Eq. (34).

In order to fit the Raman spectra in the normal state, one sees from Eqs. (32) and (35) that a great deal of parameters are required. A fitting procedure is now discussed that greatly reduces the number of free parameters. The first step in the procedure is to determine the bare phonon parameters  $\omega_\lambda$  and  $\Gamma_\lambda^i$ , which in principle can simply be read off from a fit to the lineshape of the phonon in the insulating state where  $g_\lambda = 0$ . While the intrinsic width of the phonon can be read off as  $\Gamma_\lambda^i = 2.5\text{cm}^{-1}$ , a problem arises with the position of the  $B_{1g}$  phonon, since it shows only a small renormalization with doping from the insulator to the metallic state [18], the origin of which is unknown. This could be due in part to changes of the lattice parameters with doping and/or the tetragonal to orthorhombic transition [5]. Therefore, we thus must keep this parameter free and use the bare frequency we obtain from fitting the normal state. While in principle  $g_{p-p}$  can be determined as well at this stage, since the intensity of the spectra is given in arbitrary units, this parameter (which sets the overall intensity) must also remain free.

Turning next to the metallic state, the continuum parameters  $\alpha, \beta'$ , and  $\gamma_\lambda$  are tuned to fit the full frequency range of the continuum minus the contribution of the phonons. We then tune the renormalized phonon position,  $\hat{\omega}_{B_{1g}}$ , which we later can compare with the result predicted from the value of  $g_{B_{1g}}$  obtained in Section II. Thus the only unknown parameters

are  $g_{p-p}$  (and thus  $\beta$ ), which also sets the antiresonance position  $\omega_a$ , and the bare phonon frequency.

With these constraints, such a procedure produces the theory lines shown in Fig. (4a) compared to the data of Ref. [19] on YBCO. The parameters used to obtain the fit are as follows:  $\omega_{B_{1g}} = 358\text{cm}^{-1}$ ,  $\hat{\omega}_{B_{1g}} = 348\text{ cm}^{-1}$ ,  $\Gamma_{B_{1g}} = 4.9\text{ cm}^{-1}$ ,  $\Gamma_{B_{1g}}^i = 2.5\text{ cm}^{-1}$ ,  $\alpha = 0.55$ ,  $\beta' = 3.3$ ,  $g_{B_{1g}}^2 N_F / \omega_{B_{1g}} = 0.0624$ ,  $\tau_{B_{1g}}^{*-1} = 600\text{ cm}^{-1}$ ,  $\omega_c = 12,000\text{cm}^{-1}$ , and  $g_{p-p} / \gamma_{B_{1g}} = 0.0026$ , which sets  $\omega_a = 360\text{ cm}^{-1}$ . Similar fits have been obtained before via the usual Fano expression [20,5] albeit with unconstrained parameters determined solely via a fitting routine. The value of the coupling constant used is roughly 20 percent smaller than the one given by the crude approximation in Section II. Given the uncertainty involved in the band parameters and the neglect of screening (which will reduce the crystal field and thus lower the coupling constant), we remark that the coupling constant derived from a microscopic picture of charge transfer within the unit cell provides an accurate description of the strength of the asymmetric Fano lineshape of the  $B_{1g}$  phonon in YBCO.

#### IV. SUPERCONDUCTING STATE

Turning now to the superconducting state, we note that Eq. (32) is still a valid description of the Raman lineshape provided that we use the Raman susceptibility calculated for the superconducting case. In fact, it is possible to obtain important information about the symmetry of the electron pairing in a superconductor through an investigation of the changes in the phonon lineshape below  $T_c$ . In particular, the electron-phonon coupling depends crucially on the symmetries of both the phonon and the order parameter. The role of the coupling between a phonon of given symmetry and an order parameter of a different symmetry was recently discussed by one of the authors [3], where it was shown that changes in the phonon lineshape are the greatest for a phonon which possesses the same symmetry as the order parameter while smaller changes are predicted for phonons of a symmetry orthogonal to that of the energy gap. This is pictorially shown in Fig. 2, which shows the energy gap  $\Delta(\mathbf{k})$  squared and the electron-phonon vertex  $g(\mathbf{k})$  squared, which enters into the Raman response function  $\chi$  as a weighted average around the Fermi surface. Thus the phonon vertex and the energy gap will constructively (destructively) interfere with each other if they have the same (orthogonal) symmetry. This fact can be used to determine the predominant energy gap symmetry.

In Ref. [2] the electronic contribution to Raman scattering  $\chi_\lambda$  was calculated in detail for

a superconductor with  $d_{x^2-y^2}$  pairing symmetry and good fits were obtained to the Raman spectra of BSCCO. For details of the theory, we direct the reader to that Reference and simply write down the Raman response function obtained for the  $B_{1g}$  channel using a  $d_{x^2-y^2}$  gap,  $\Delta(\hat{\mathbf{k}}, T) = \Delta_0(T) \cos(2\varphi)$  for a cylindrical Fermi surface (here  $x = \omega/\Delta_0$ ):

$$\chi''_{B_{1g}} = \tanh(\omega/4T) \frac{2N_F}{3\pi x} \begin{cases} [(2+x^2)K(x) - 2(1+x^2)E(x)], & x \leq 1, \\ x[(1+2x^2)K(1/x) - 2(1+x^2)E(1/x)], & x > 1. \end{cases} \quad (36)$$

The real parts are obtainable through Kramers-Kronig analysis (see Ref. [3]). The resulting response has a logarithmic divergence at the pair edge (an artifact of the two-dimensional nature of the Fermi surface) and vanishes as  $x^3$  for small frequencies. To make a fit to the continuum in the superconducting state, we first convolute Eq. (36) with a Gaussian to mimic the effect of finite  $z$  dispersion of the Fermi surface, experimental resolution, etc. Fitting the resulting function to the superconducting state continuum for YBCO leads to value  $\Delta = 240 \text{ cm}^{-1}$  and a smearing width  $\Gamma/\Delta = 0.2$  (not to be confused with the intrinsic phonon linewidth). Then, Eq. (36) can be used to draw a fit to the full  $B_{1g}$  response using the parameters obtained from the fit to the response in the normal metal.

The resulting fit to the lineshape using Eq. (36) and its corresponding real part (determined via Kramer's Kronig transformation) at  $T = 20K$  is shown in Fig. (4b) compared to the data on YBCO from Ref. [21]. Here the parameters used are the same as in the normal metal case (Section III) with the only change resulting in the use of Eq. (36) and its real part rather than Eqs. (34-35). Using the coupling constant  $\lambda = 0.0624$  as obtained in fitting the normal state leads to  $\hat{\omega}_{B_{1g}} = 337 \text{ cm}^{-1}$  and  $\Gamma_{B_{1g}} = 7.9 \text{ cm}^{-1}$ , i.e., the phonon broadens and softens at low temperatures compared to its normal state lineshape.

The fit points towards the predominance of an energy gap of  $B_{1g}$  symmetry for the following reasons. First we remark that the theory predicts the correct magnitude and sign of the phonon renormalization due to superconductivity. This would be in marked contrast if the gap was  $s$ -wave or of  $d$ -wave nature but of other symmetry ( $d_{xy}, d_{3z^2-r^2}$ , etc). In the first case an isotropic gap would lead to trivial coupling of the energy gap to the symmetry of the phonon and all phonons would show the same qualitative behavior, which is not the case for the cuprates [5]. In the second case, previous work has demonstrated that the channel probed via Raman scattering which shows a peak at the highest frequency in the continuum in the superconducting state of all the channels gives the predominant symmetry of the energy gap. This again points to  $d_{x^2-y^2}$  pairing. Further, if the gap was of another symmetry (i.e.,  $B_{2g}$  or  $A_{1g}$ ) then the position of the phonon,  $\omega_{B_{1g}}/\Delta = 1.42$ , would predict small phonon softening since (i) the real part of the phonon self energy changes from negative

to positive values at roughly  $\omega/\Delta = 1.5$ , and (ii) the weight  $\langle \gamma^2(\mathbf{k}) | \Delta(\mathbf{k})|^2 \rangle$  over the Fermi surface which determines the coupling would be smaller for a gap of different symmetry than the vertex. Therefore, while although Raman cannot distinguish between and energy gap which changes sign or not around the Fermi surface, the evidence from the data indicate that the electronic pairing is predominantly of  $d_{x^2-y^2}$  symmetry.

## V. CONCLUSIONS

In order to improve the study of the superconducting gap anisotropy in high temperature superconductors [2,3] the interactions of the electronic continuum and the characteristic phonons shown in Fig. 1 have been included in the theory. These interactions and the intrinsic width of the phonons had complicated a previous comparison of the theory for the continuum for certain gap anisotropy to the experimental data since the contribution of the phonons had to be subtracted in an intuitive way (see Ref. 2). In addition, the phonon lineshape is of course distorted by the Fano interference.

The starting point of our calculation was the model calculation of the electron-phonon interaction based on Ref. 6 and a simple tight binding calculation for the electrons is used. The latter is certainly not very adequate but demonstrates the correct characteristic symmetry properties of the electronic wave functions.

Our main conclusions are as follows:

(i) *Phonon lineshape* - The asymmetric Fano lineshape of the  $B_{1g}$  phonon is reproduced while the interaction of the continuum with the  $A_{1g}$  phonon is much weaker according to the experiments [5] and disappears in our model calculation (see Sec. II B). Using more adequate electronic wave functions, this coupling may reappear but still must be weaker than in the case of the  $B_{1g}$  phonon;

(ii) *Electric Field* - The perpendicular electric field acting on the oxygen atoms in the  $\text{CuO}_2$  plane has been determined by a comparison with the experiments in the normal phase, assuming tetragonal symmetry, i.e.,  $\vec{E} = \vec{E}_x = \vec{E}_y$ . This symmetry is certainly destroyed by the presence of the chains as shown in Fig. 1, and results in a mixing of the  $A_{1g}$  and  $B_{1g}$  symmetry channels. It is obvious from the coupling presented in Sec. II B and from the calculation of the diagrams depicted in Fig. 3, that starting with, e.g., light polarizations assigned to  $B_{1g}$  symmetry, the coupling with  $\vec{E}_x \neq \vec{E}_y$  leads to a contribution to the electronic continuum of  $A_{1g}$  symmetry which is further coupled to the  $A_{1g}$  phonons. The  $A_{1g}$  phonons do appear in the  $B_{1g}$  spectrum observed by experiments (see Fig. 4a),

but it is not clear whether this is dominantly due to misalignments of the samples or to the channel mixing. A more elaborate calculation of the electric fields  $\vec{E}_x$  and  $\vec{E}_y$  arising from different ions would certainly help to resolve this question;

(iii) *Gap anisotropy* - The excellent fit of the combined electronic continuum + phonon spectrum in Fig. 4b is obtained by assuming the simplest form of the superconducting gap of  $d_{x^2-y^2}$  type for  $B_{1g}$  symmetry. The parameters are borrowed from the fitting of the normal state. The only additional parameters introduced are the gap amplitude defined above Eq. (36) and an additional smearing  $\Gamma \sim 0.2\Delta_0$  with a non-unique origin (see Sec. IV). This fit certainly supports the previous fit in Ref. [2] where the phonons had been subtracted.

Concerning the anisotropy of the gap it has already been pointed out that Raman scattering provides information only concerning the absolute value of the gap. The fit of the low energy spectra in the present paper clearly demonstrates that assuming  $d$ -wave pairing in the superconductor, the gap with  $d_{x^2-y^2}$  symmetry gives an excellent fit but  $d_{xy}$ ,  $d_{xz}$ , and  $d_{yz}$  are not applicable (see e.g., Ref. [2]). A very highly anisotropic extended  $s$ -wave state which has predominantly  $B_{1g}$  symmetry cannot be ruled out.

For instance recently the photoemission experiment of Ref. [22] suggests a gap which can be represented by the form  $\Delta(\varphi) = \Delta_0[1 + a \cos(4\varphi)]/(1 + a)$ , with the parameter  $a$  just exceeding one. Our fits clearly show that a fit with  $a = 1$  are not satisfactory. The reason is that the different contributions of the different gap features to the low energy ( $\omega \ll \Delta_0$ ) part of the spectra with e.g.  $B_{1g}$  symmetry: (i) the large gap around  $\varphi = \frac{\pi}{2}n$ , ( $n = 0, 1, 2, \dots$ ) does not contribute (see Fig. 2); (ii) the gap changing sign at  $\varphi = \frac{\pi}{4} + n\frac{\pi}{2}$  contributes as  $\omega^3$  at low frequencies; (iii) the gap touching zero with zero slope (parameter  $a = 1$ ) at  $\varphi = \frac{\pi}{4} + n\frac{\pi}{2}$  contributes as  $\omega$  at low frequencies (see Ref. [2]); (iv) the gap with zero slope but not at zero energy (parameter  $a \neq 1$ ) gives a sharp discontinuity and approximately linear term (modulo logs) above or below it ( $a < 1$  and  $a > 1$ , respectively).

On the basis of the above features, the zero slope at energy larger than  $\sim 20\text{cm}^{-1}$  and at  $\varphi = \frac{\pi}{4} + n\frac{\pi}{2}$  can be ruled out. Any feature with a gap minimum on a smaller energy scale can however still be possible, but the region of the Fermi surface where the minima occur must be very narrow compared with those given by the expression mentioned above. As the minima should occur in an anomalously narrow region, the slopes coming or leaving the minima must be very large. Such a behavior appear to us as very unlikely.

In summary, the main result of the present paper is the confirmation of the conclusion of Refs. [2,3], namely, that the Raman spectra are in excellent agreement with a superconducting gap of  $d_{x^2-y^2}$  symmetry, but gaps with very sharp features on a small part of the

Fermi surface cannot be ruled out.

### **ACKNOWLEDGMENTS**

The authors would like to acknowledge stimulating discussions with G. T. Zimányi, B. Stadlober, D. Reznik, R. Hackl, J. C. Irwin, D. Einzel, and M. Cardona. One of the authors (T.P.D.) would like to acknowledge the hospitality of the Research Institute for Solid State Physics of the Hungarian Academy of Science and the Institute of Physics of the Technical University of Budapest where parts of this work were completed. This work was supported by the US-Hungarian Science and Technology Joint Fund under Project No. 265, NSF Grant number 92-06023, and by the Hungarian National Research Fund under Grants No. OTKA2950, 7283 and T4473.

## REFERENCES

- [1] A. Sokol and D. Pines, Phys. Rev. Lett. **71**, 2813 (1993); S. Chakravarty, A. Sudbø, P. W. Anderson, and S. Strong, Science **251**, 337 (1993); N. Bulut, D. J. Scalapino, and S. R. White, Phys. Rev. B **47**, 6157 (1993).
- [2] T. P. Devereaux *et.al.*, Phys. Rev. Lett. **72**, 396 (1994), and *ibid.* **72**, 3291 (1994).
- [3] The effect of the electronic continuum on the phonons of different symmetry has recently been studied by T. P. Devereaux (to appear in Phys. Rev. B) without using a definite model for the electron-phonon coupling and examining the Raman lineshape.
- [4] S. L. Cooper *et.al.*, Phys. Rev. B **38**, 11934 (1988).
- [5] see e.g. C. Thomsen, in *Light Scattering in Solids VI*, edited by M. Cardona and G. Güntherodt (Springer, Berlin, 1991).
- [6] S. Barišić and I. Kupčić in *High Temperature Superconductivity*, Vol. 23, *Strongly Correlated Electron Systems I.*, eds. G. Baskaran, A. E. Ruckenstein, E. Tosatti, and Yu Lu (World Scientific, Singapore, 1990), p. 325.
- [7] S. Barišić and I. Batistić, Europhys. Lett. **8**, 765 (1989).
- [8] H. Monien and A. Zawadowski, Phys. Rev. Lett. **63**, 911 (1989).
- [9] M. V. Klein and S. B. Dierker, Phys. Rev. B **29**, 4976 (1984); H. Monien and A. Zawadowski, Phys. Rev. B **41**, 8798 (1990).
- [10] V. G. Hadjiev *et.al.*, Sol. State Comm. **80**, 643 (1991).
- [11] A. Zawadowski, Physica Scripta **T27**, 66 (1989).
- [12] See eg.: N. W. Ashcroft and N. D. Mermin, *Solid State Physics* (Saunders College, Philadelphia, 1976), p. 780.
- [13] P. B. Allen, Phys. Rev. B **13**, 1416 (1976).
- [14] If the ratio of the copper and oxygen displacements of the  $A_{1g}$  mode is denoted by  $\delta_{Cu}$ , we obtain instead of Eq.(26)

$$g_{A_{1g}}(\mathbf{k}, \mathbf{q} = 0) = eE_z \sqrt{\frac{\hbar}{2M_o\omega_{A_{1g}}}} \frac{1}{\sqrt{2+\delta_{Cu}^2 M_{Cu}/M_o}} \times [|\phi_x(\mathbf{k})|^2 + |\phi_y(\mathbf{k})|^2 - \delta_{Cu}|\phi_b(\mathbf{k})|^2(\mathbf{E}_b)_z/E_z].$$

Since  $\phi_b(\mathbf{k}) = \text{const.}$  on the Fermi surface (see Eq.(16a)), even the above more accurate expression does not yield significant (unscreened) coupling.

[15] More specifically,

$$\chi_\lambda(\mathbf{q}, i\omega) = \sum_{\mathbf{k}, \mathbf{p}} \phi_\lambda(\mathbf{k}) [i\omega \Phi_{\mathbf{k}, \mathbf{p}}(\mathbf{q}, i\omega) + g(\mathbf{q})] \phi_\lambda(\mathbf{p}),$$

where  $\phi_\lambda$  are Fermi surface harmonics in channel  $\lambda$ ,  $\Phi$  is the phase-space density Kubo function, and  $g$  is the wavevector dependent compressibility, [see, e.g., D. Forster, *Hydrodynamic Fluctuations, Broken Symmetry, and Correlation Functions* (Benjamin, New York, 1975)].

[16] A. Zawadowski and M. Cardona, Phys. Rev. B **42**, 10 732 (1990).

[17] A. Virosztek and J. Ruvalds, Phys. Rev. B **45**, 347 (1992).

[18] D. Reznik *et. al.*, Phys. Rev. B **48**, 7624 (1993).

[19] T. Staufer, R. Hackl, and P. Müller, Solid State Comm. **75**, 975 (1990); *ibid.* **79**, 409 (1991).

[20] G. Blumberg *et. al*, Journ. of Supercond. **7**, 445 (1994) and references therein.

[21] R. Hackl *et. al.*, Phys. Rev. B **38**, 7133 (1988).

[22] J. C. Campuzano *et. al.*, private communication.

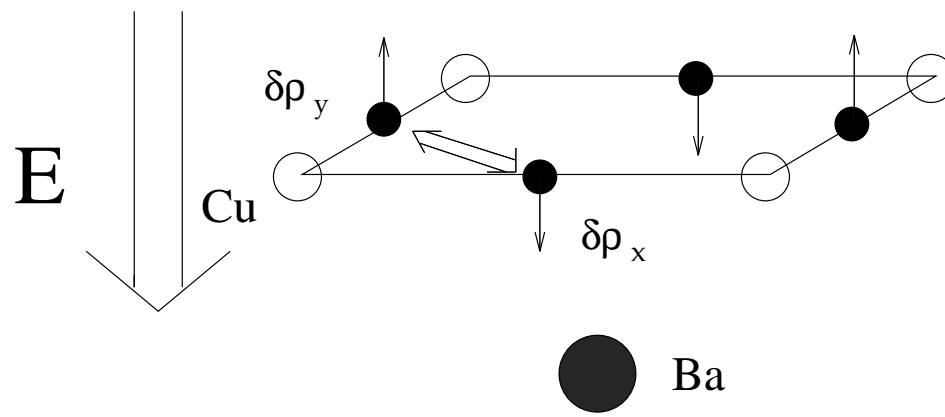
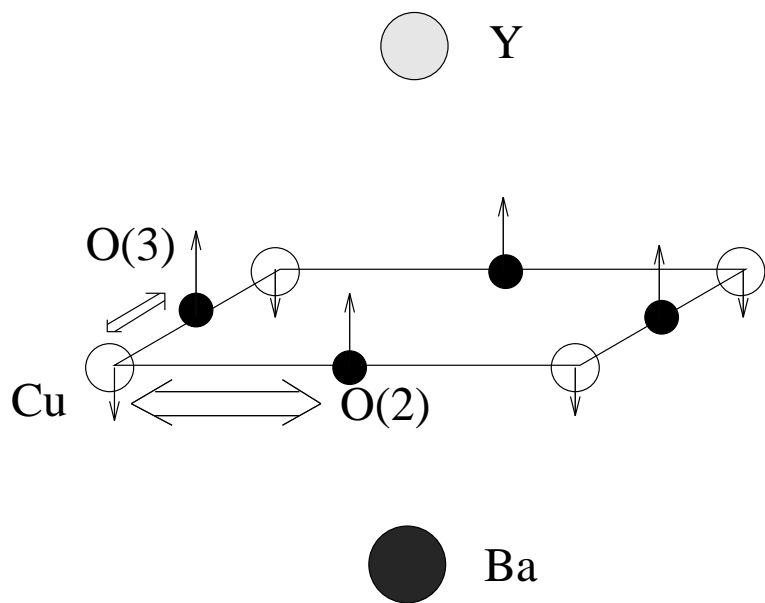
## FIGURES

FIG. 1. The unit cell of the  $\text{CuO}_2$  plane in  $\text{YBa}_2\text{Cu}_3\text{O}_y$  is shown with the atomic displacements corresponding to the phonons of  $A_{1g}$  (a.) and  $B_{1g}$  (b.) symmetry. A finite electric field  $\mathbf{E}$  perpendicular to the planes due to the asymmetric environment (Y above, Ba below) is indicated. This induces the respective charge transfer fluctuations ( $\delta\rho$ ) denoted by the two way arrows.

FIG. 2. The dashed line above the cylindrical Fermi surface (F.S.) represents a  $d_{x^2-y^2}$  superconducting gap  $|\Delta(\phi)|^2 \sim \cos^2(2\phi)$ . The areas shaded by the vertical dotted lines mark the regions of the F.S. which are probed by Raman scattering in the  $A_{1g}$  (a.) and in the  $B_{1g}$  (b.) geometries.

FIG. 3. Feynman diagrams depicting the three contributions to Raman scattering in metals. Here the solid line is the electron Green's function, the wavy line the phonon propagator, and the dashed line the photon propagator. The vertices are defined as in the text.

FIG. 4. (a).Fit of Eq. (32), (34-35) to the  $B_{1g}$  spectra from Reference [19] on YBCO at  $T = 100K$ . The parameters used to obtain the fit are discussed in the text;(b) Fit of Eqs. (32) and (36) to the  $B_{1g}$  spectra from Reference [21] on YBCO at  $T = 20K$ . The parameters used to obtain the fit are discussed in the text. The additional phonons besides the  $340 \text{ cm}^{-1}$  have been subtracted off for clarity (see Fig. 4a).



$A_{1g}$

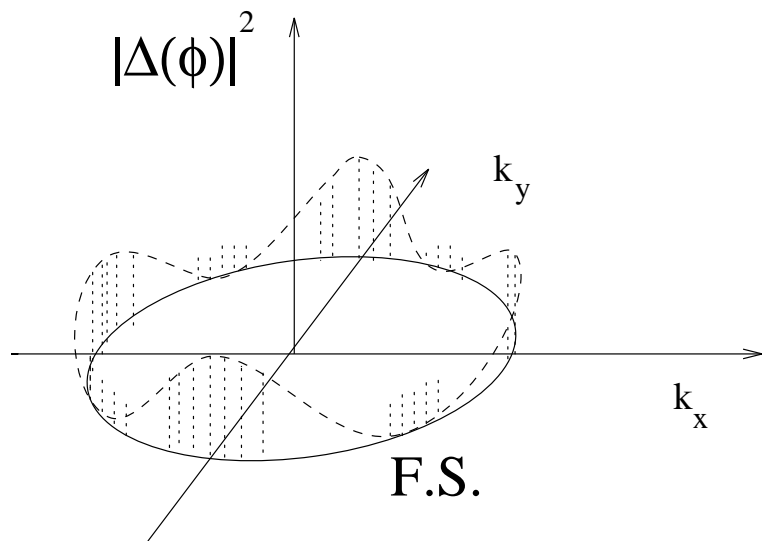
a.



$B_{1g}$

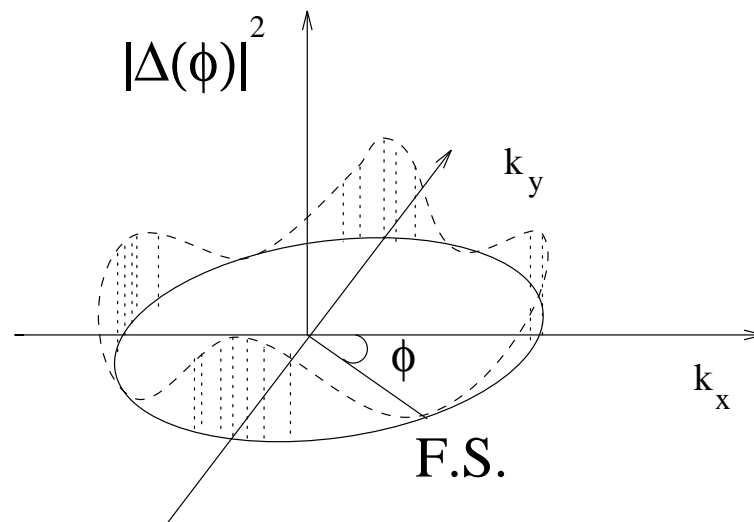
b.

Devereaux et. al. Fig 1.



$A_{1g}$

a.



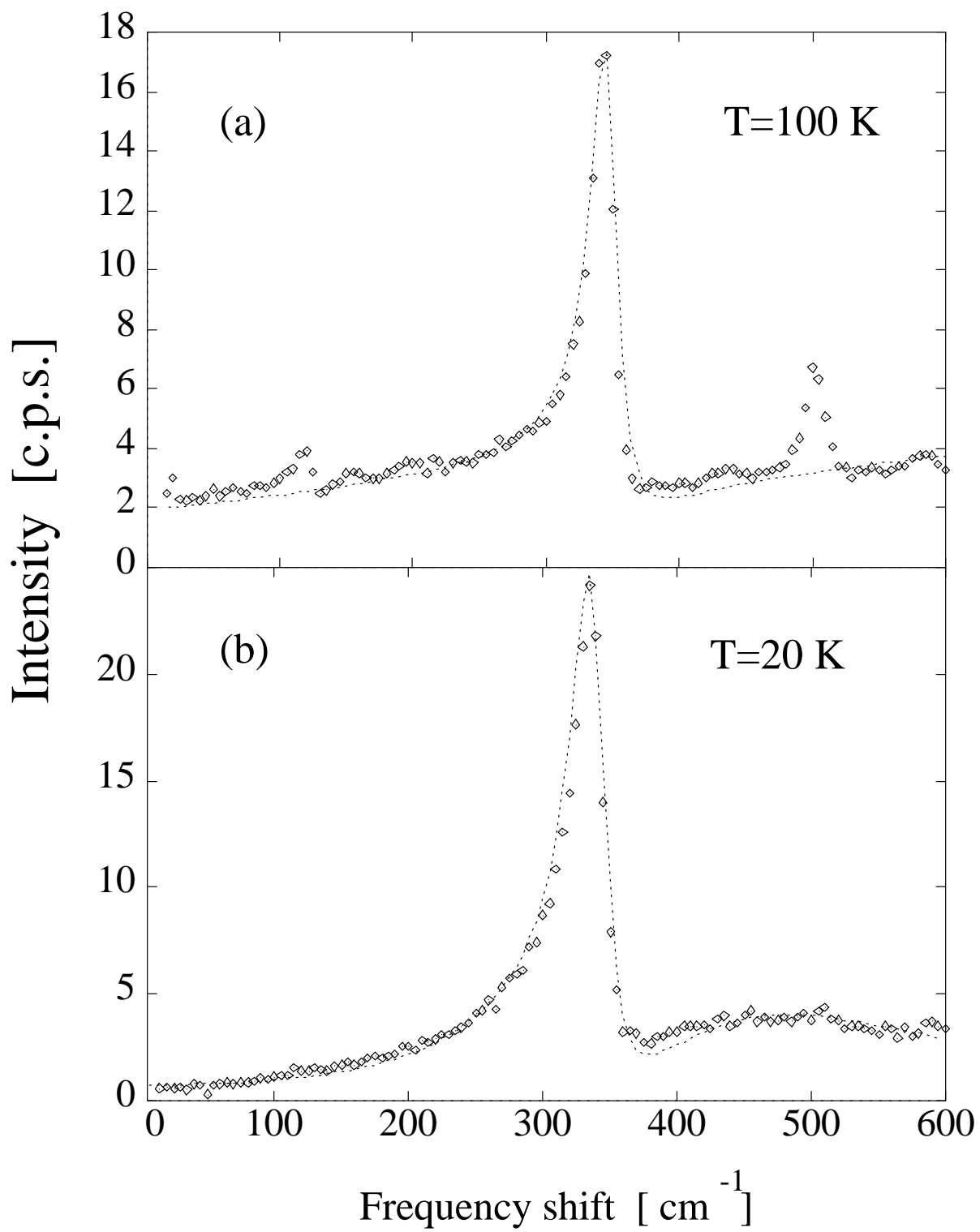
$B_{1g}$

b.

Devereaux et. al. Fig. 2

$$\begin{aligned}
\chi_{full}(\omega) = & \gamma \left[ \text{loop} + \text{loop} \otimes \text{loop} + \dots \right] \\
& + 2 g_{p-p} \left[ \text{loop} + \text{loop} \otimes \text{loop} + \dots \right] \\
& + g_{p-p} \left[ \text{loop} + \text{loop} \otimes \text{loop} + \dots \right]
\end{aligned}$$

Devereaux et. al. Fig. 3



Devereaux et. al. Fig. 4